Atom Location by Axial-Electron-Channeling Analysis

S. J. Pennycook and J. Narayan[(a)]
Solid State Division, Oak Ridge National Laboratory, Oak Ridge, Tennessee 37831
(Received 27 September 1984)

The channeling of electrons along or between atomic rows in a crystal is used as the basis of a powerful lattice-location technique capable of analyzing small quantities of crystal impurities with high spatial resolution. We demonstrate the technique by locating Sb dopant in Si and compare the results with ion-channeling and planar-electron-channeling analysis. Delocalization corrections are required with the electron-channeling analyses.

PACS numbers: 61.80.Mk, 61.70.Wp

Axial-electron-channeling analysis is a new quantitative technique for determining the lattice location of dopant or impurity atoms from small regions of a crystal examined by a transmission electron microscope (TEM). The analysis used the strong variation in characteristic x-ray intensity seen for small changes in crystal orientation close to a zone axis. The effects are much larger than with planar-channeling analysis,[1,2] allowing higher sensitivity and much more convenient lattice-location analysis. Two or more sets of planes are used to set up standing waves in several directions simultaneously and channel the electron current into columns. These columns may be located on the atomic strings of the crystal, or in various positions in between, forming a powerful new technique for lattice-location analysis. A similar advantage of axial geometry is seen in the closely related technique of ion-channeling analysis.[3]

Figure 1 shows the computed electron intensity at the exit surface of a (001) Si crystal in two orientations at various thicknesses, with the bright areas corresponding to high intensity. For each orientation the intensity scale is normalized to the peak intensity encountered, and the projected potential is shown to mark the atom sites. The calculation was performed by a multislice program using 41 diffracted beams.[4] Figure 1(a) shows the case with the electron beam incident exactly long [001], when the current is well channeled down the columns of Si atoms. The peak intensity is approximately six times the mean intensity, and shows a spatial periodicity along the channel of approximately 25 nm. In Fig. 1(b), the incident beam is tilted just outside the exact Bragg orientation of (220) and $(\bar{2}20)$ planes, when the current is channeled between the columns of Si atoms. The peak intensities are only three times the mean intensity, and well-formed peaks occur approximately every 12.5 nm in depth, although the position of these peaks varies somewhat along the direction of beam tilt. Figure 2 shows that a similar situation occurs for a (111) orientation. When the beam is incident exactly along [111], the current is again well channeled along the strings of atoms [Fig. 2(a)], although the peak intensities are now ten times the mean. With the beam incident outside the {220}-reflecting positions the current is channeled between the atom strings, with a peak intensity of only three times the mean [Fig. 2(b)].

For an experimental lattice-location analysis, it is

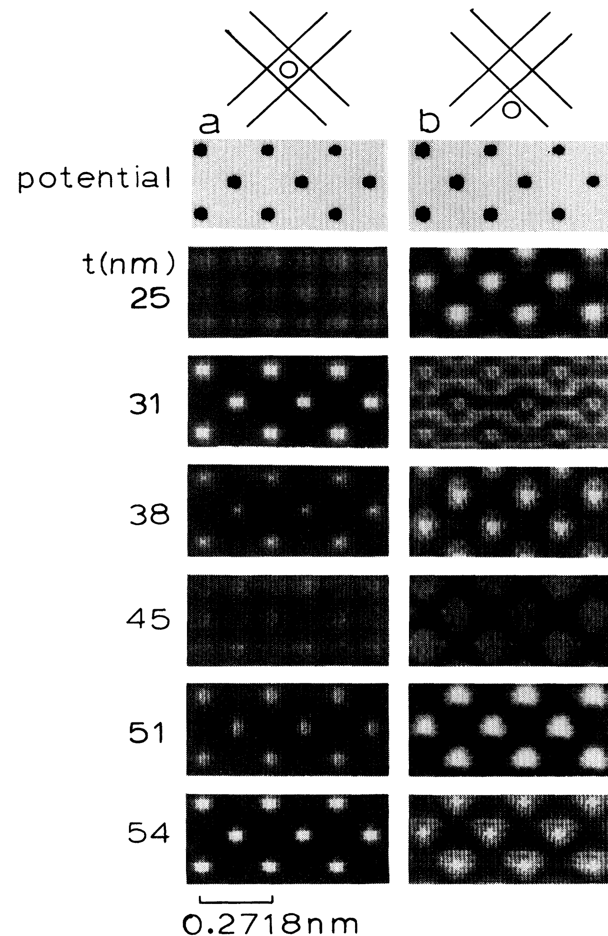

FIG. 1. Electron current distributions for ⟨100⟩ axial-channeling analysis in Si at various thicknesses (t) of crystal with the two incident beam orientations shown schematically.

© 1985 The American Physical Society

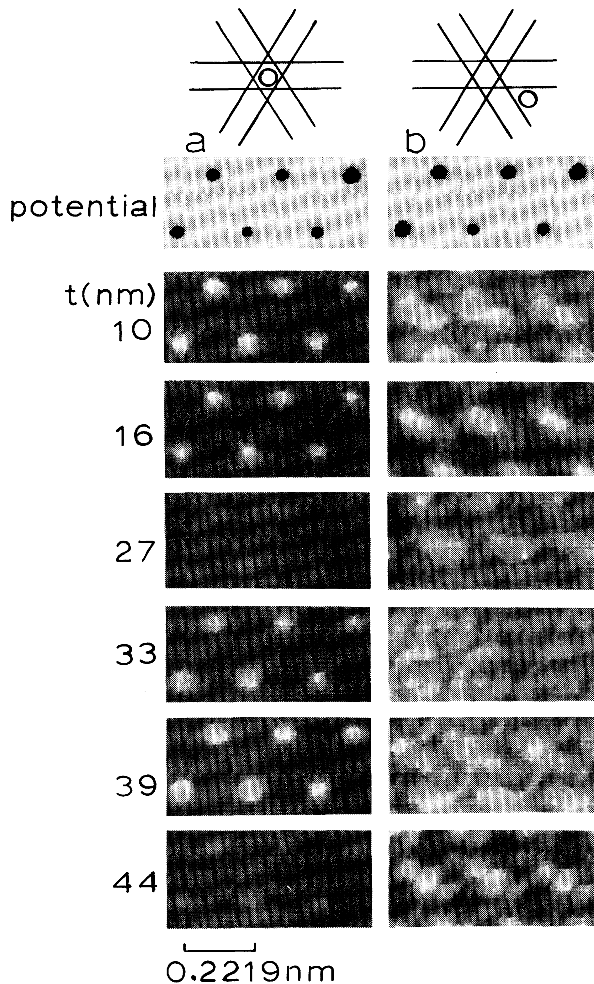

FIG. 2. Electron current distributions for ⟨111⟩ axial-channeling analysis in Si.

not necessary to calculate these detailed current distributions. A simple ratio technique is used in which the matrix x-ray intensity monitors the thickness-integrated electron current down the matrix atomic strings. Since the current distribution changes with thickness, the impurity must be distributed uniformly through the sample (although in practice only small errors may be introduced by a nonuniform distribution).[5] For this study, the near-surface region of a {100} Si sample was alloyed with Sb by a laser-melting procedure[6] to give an Sb concentration of approximately 2 at.% in the top 200 nm of the sample. An ion-channeling analysis is given in Fig. 3, showing the alloy to be 97% substitutional, except for a small band of high concentration near the surface.[7] A cross-section TEM sample was prepared by an ion-milling technique, which allowed the ⟨100⟩ and ⟨111⟩ axes to be reached in the same specimen, and ensured a uniform distribution of dopant through the sample thickness. Figure 4(a) shows a TEM cross-section image using diffraction constrast, which shows that the alloyed region is free of extended defects. Figure 4(b) shows an image taken by scanning transmission electron microscopy using Z contrast[8] which shows directly the extent of the dopant.

Electron-channeling analyses were performed on areas 100 nm in diameter within the band of dopant, and approximately 100 nm in thickness. Figure 5 shows a comparison of x-ray spectra obtained for {220} planar and ⟨100⟩ and ⟨111⟩ axial channeling; all of the data were taken with the same incident beam current. Substantially enhanced x-ray yields occur with the beam incident along a zone axis, the ⟨111⟩ axis giving greater enhancement than the ⟨100⟩ axis, consistent with the computed peak intensities. A comparison of the typical x-ray yield variations ΔX is given in Table I for {220} and {400} planar-,[2] and ⟨100⟩ and ⟨111⟩ axial-channeling conditions. It can be seen that a rough estimate of the axial yield variation is given by the product of the yield variations for the lowest-order planes contained in the zone axis; thus $\Delta X^{\langle 100\rangle} \approx \Delta X^{\{220\},2}$ and $\Delta X^{\langle 111\rangle} \approx \Delta X^{\{220\},3}$ although the exact yield variations seen in practice depend on the exact incident beam directions and convergence and the local sample thickness.

The quantitative determination of the substitutional fraction F_s is very straightforward if the excitations of the inner-shell electrons of impurity and matrix atoms are sufficiently localized. F_s is then simply given by the ratio of the channeling effects. If ΔX_{Sb} is the ratio of the Sb x-ray intensity, and ΔX_{Si} the ratio of the Si x-ray intensity in the two channeling orientations, then

$$F_s = (\Delta X_{\mathrm{Sb}} - 1)/(\Delta X_{\mathrm{Si}} - 1). \qquad (1)$$

However, in this case it was found that the excitations, although highly localized, were not both sufficiently localized for this expression to give agreement with the ion-channeling analysis. We can estimate the localization of the excitations as follows. A fast electron of velocity v can transfer energy ΔE to a crystal electron if it passes closer than a cutoff distance b given by[9]

$$b = \hbar v/\Delta E. \qquad (2)$$

This expression is the limiting case for small-angle scattering but many x rays are generated as a result of large-angle scattering events which are more highly localized. A mean-square-average impact parameter can be obtained by use of $b = 1/q$, where q is the momentum transfer, and integration over all scattering angles,[10] given by

$$b^{\mathrm{rms}} = (\bar{h} v/\Delta E)[\ln(4E/\Delta E)]^{-1/2}, \qquad (3)$$

where E is the incident beam energy, and ΔE is now the inner-shell binding energy. For 100-keV elec-

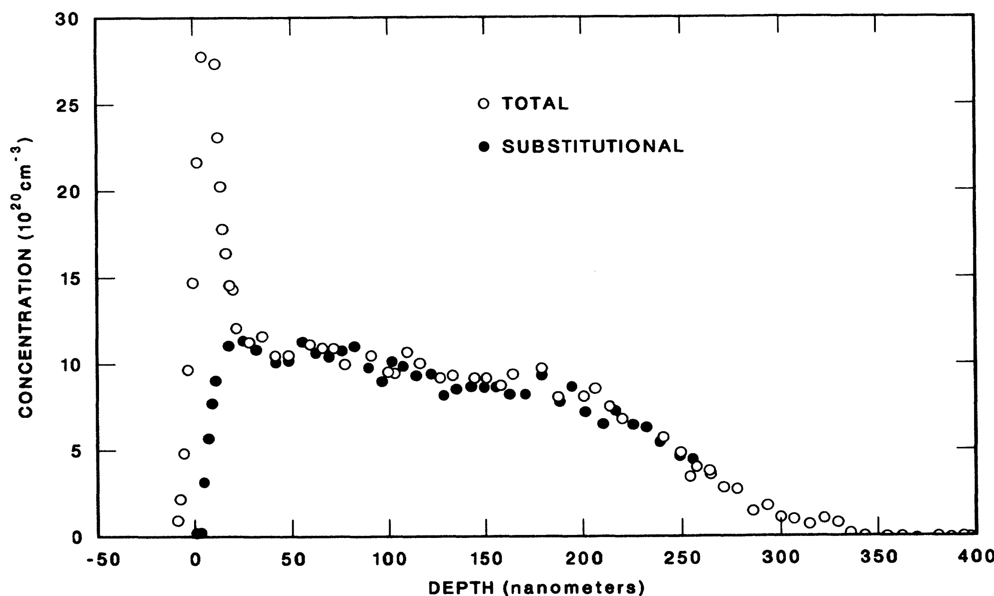

FIG. 3. Bulk ion-channeling analysis of Si-Sb alloy.

trons, we find $b_{\mathrm{Sb}}^{\mathrm{rms}} = 0.0138$ nm $< b_{\mathrm{Si}}^{\mathrm{rms}} = 0.0266$ nm. While both are small compared to the {220} interplanar spacing of $d = 0.192$ nm, so that both x-ray intensities show good channeling effects, the greater localization of the Sb excitation leads to a yield variation slightly greater than for Si. To take account of this difference in localization of impurity and matrix excitations, we define

$$F_s = (1/C)(\Delta X_{\mathrm{Sb}} - 1)/(\Delta X_{\mathrm{Si}} - 1), \quad (4)$$

where C is a delocalization correction factor to be determined experimentally at present. In {220} planar channeling of a Si-Sb alloy, it was found experimentally that agreement with the ion-channeling analysis was obtained with $C = 1.10 \pm 0.04$.[2] In the $\langle 100 \rangle$ axial channeling, we found $C = 1.04 \pm 0.03$. The lower value is presumably because the peak in the electron current is moved a larger distance from the atom site in the axial geometry compared to planar geometry, $0.71d$ compared to $0.5d$, respectively. This simulates a larger interplanar spacing when delocalization effects

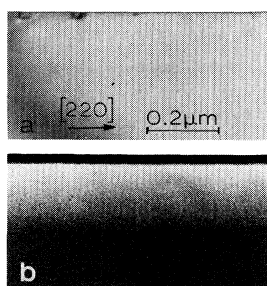

FIG. 4. Cross-section images of Si-Sb alloy. (a) TEM image showing Si structure, (b) Z-contrast scanning transmission electron microscopy image showing dopant distribution.

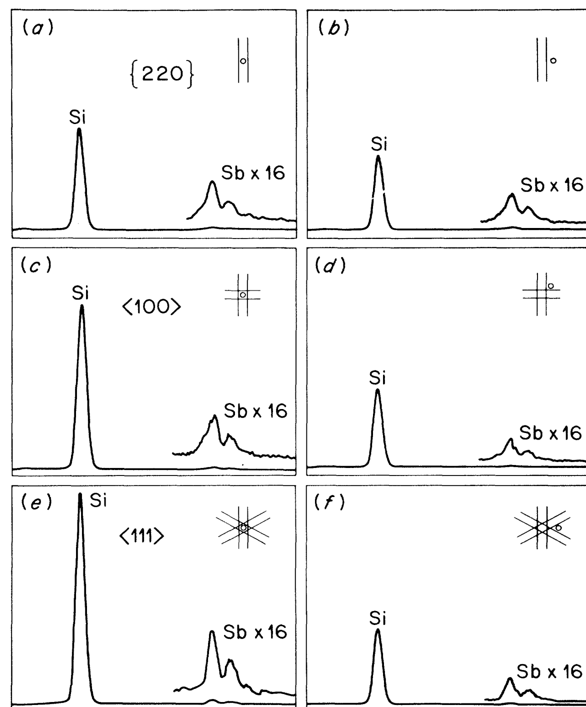

FIG. 5. X-ray spectra obtained for {220} planar- and $\langle 100 \rangle$ and $\langle 111 \rangle$ axial- electron-channeling analysis.

TABLE I. Typical Si x-ray yield variations seen for various channeling conditions, and the corresponding delocalization correction factors C for Sb-atom location.

Channeling condition	ΔX_{Si}	C
{220} planar	1.4	1.10 ± 0.04
{400} planar	1.2	1.17 ± 0.07
⟨100⟩ axial	2.2	1.04 ± 0.03
⟨111⟩ axial	3.1	1.05 ± 0.02

are reduced, so that the Sb and Si yield variations are more equal and also larger. For ⟨111⟩ axial channeling, where the peak electron current is moved by $0.67d$, we found $C = 1.05 \pm 0.02$ (see Table I).

The minimum area which can be analyzed by axial channeling is somewhat larger than the smallest available electron probes since a collimated electron beam is required. The results described here were obtained with use of a probe convergence semiangle of 3.4 mrad, approximately one-third of the Bragg angle for a {220} reflection, resulting in an Airy disk pattern with a full width at half maximum of approximately three {220} spacings, or 0.6 nm. Probe spreading due to spherical aberration of the objective lens is small at such convergence angles. It must also be remembered that the ratio technique described here is only accurate for a uniform depth distribution of dopant. High-resolution analysis around extended defects can be achieved by tilting the defect so that its plane, or line, is parallel to the beam, and using samples thin enough that the defects run through the whole sample thickness. Such techniques are routinely used for high-resolution imaging studies.

In conclusion, it has been shown that an axial-channeling geometry can be used to channel the electron current down or between atomic columns to give a larger variation of impurity and matrix characteristic x-ray emission with incident beam orientation than can be achieved by a planar-channeling geometry. Effects due to delocalization of the inner-shell excitation are reduced compared to the corresponding planar-channeling geometry. The greater sensitivity of axial channeling allows the electron-channeling analysis to be extended to situations in which lower x-ray intensities are generated, thus opening up exciting areas related to impurity precipitation and segregation at dislocations, twins, and stacking faults, which are the fundamental processes governing gettering and alloying phenomena in materials, particularly semiconductors.

The authors would like to thank E. Fogarassy, R. J. Culbertson, and D. Fathy for research collaborations, M. T. Robinson for computing assistance, and R. H. Ritchie for useful comments on the manuscript. This research was supported in part by the Division of Materials Sciences, U. S. Department of Energy under Contract No. DE-AC05-840R21400 with Martin Marietta Energy Systems, Inc.

[a]On sabbatical leave at the Microelectronics Center of North Carolina, Research Triangle Park, N.C. 27709, and the Materials Engineering Department, North Carolina State University, Raleigh, N.C. 27650.

[1]J. C. H. Spence and J. Tafto, J. Microsc. (Oxford) **130**, 147 (1983).

[2]S. J. Pennycook, J. Narayan, and O. W. Holland, Appl. Phys. Lett. **44**, 547 (1984).

[3]*Materials Analysis by Ion Channeling,* edited by L. C. Feldman, J. W. Mayer, and S. T. Picraux (Academic, New York, 1982).

[4]Computer programs supplied by the Facility for High Resolution Electron Microscopy, Arizona State University, Tempe, Arizona.

[5]S. J. Pennycook, J. Narayan, and O. W. Holland, in *Electron Microscopy of Materials,* Materials Research Society Symposia Proceedings, Vol. 31, edited by W. Krakow, D. A. Smith, and E. W. Hobbs (Elsevier/North-Holland, New York, 1984), p. 97.

[6]J. Narayan, J. Cryst. Growth **59**, 583 (1982).

[7]E. Fogarassy and J. Narayan, unpublished.

[8]S. J. Pennycook and J. Narayan, Appl. Phys. Lett. **45**, 385 (1984).

[9]J. D. Jackson, *Classical Electrodynamics* (Wiley, New York, 1975), 2nd ed., p. 623.

[10]S. J. Pennycook, Contemp. Phys. **23**, 371 (1982).

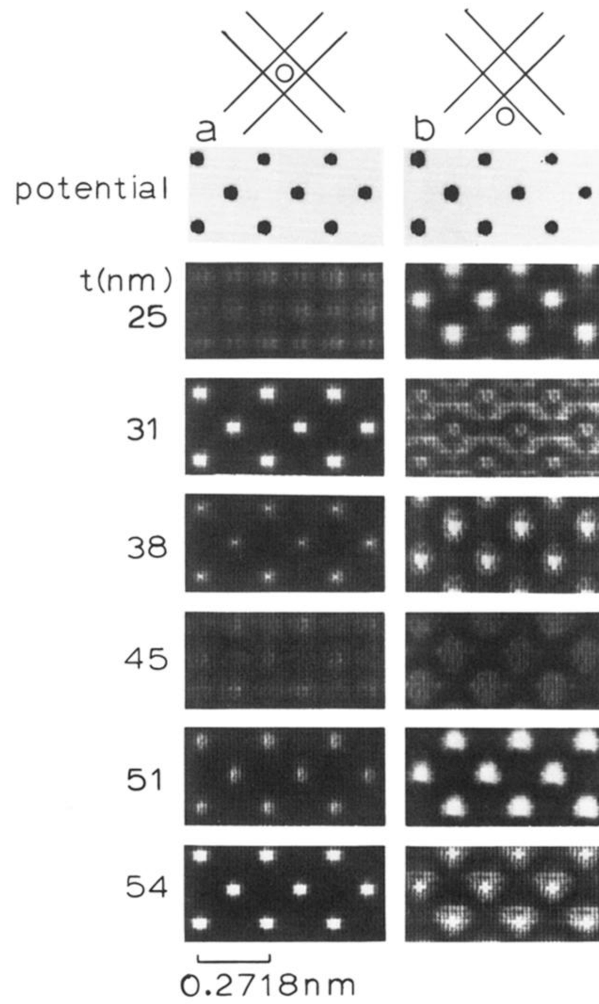

FIG. 1. Electron current distributions for ⟨100⟩ axial-channeling analysis in Si at various thicknesses (t) of crystal with the two incident beam orientations shown schematically.

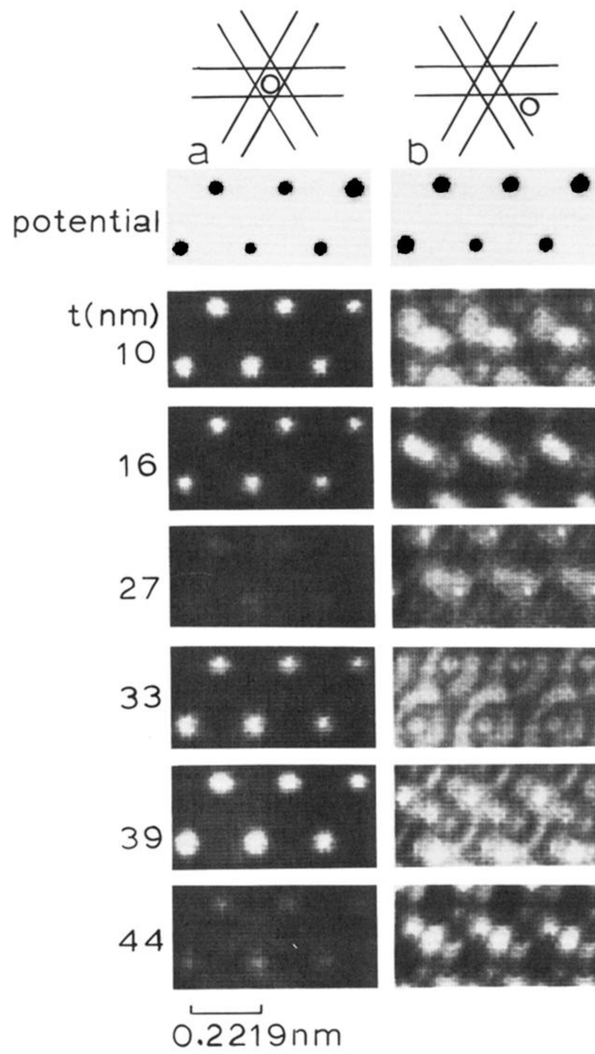

FIG. 2. Electron current distributions for ⟨111⟩ axial-channeling analysis in Si.

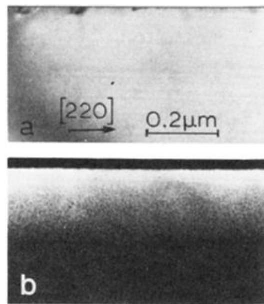

FIG. 4. Cross-section images of Si-Sb alloy. (a) TEM image showing Si structure, (b) Z-contrast scanning transmission electron microscopy image showing dopant distribution.